Fluorescence excitation spectroscopic study of the jet-cooled acetyl cyanide

Min-Chul Yoon, Young S. Choi, and Sang Kyu Kim[a)]
Department of Chemistry, Inha University, Inchon (402-751), Republic of Korea

(Received 21 October 1998; accepted 19 January 1999)

Fluorescence excitation spectrum of acetyl cyanide (CH_3COCN) in a supersonic jet has been obtained for the $^1(n,\pi^*)$ transition (S_1-S_0). A spectral origin band is located at 27 511 cm^{-1}, and its fluorescence lifetime is measured to be $3.5\pm0.3\,\mu s$. The S_1 state vibrational modes associated with CH_3 torsion, CCO bend, CCN bend, and CO wag are found to be optically active. The fluorescence intensity decreases with increasing the energy from the origin up to $\sim$2000 cm^{-1}, while the fluorescence lifetime changes little over the same energy region. Instead, a broad background signal appears in the high energy region, indicating that the intramolecular vibrational redistribution (IVR) process becomes important in the S_1 state as the density of states increases. © *1999 American Institute of Physics.* [S0021-9606(99)00515-2]

I. INTRODUCTION

Photochemistry of acetyl cyanide (or pyruvonitirile; CH_3COCN), in spite of its interesting photochemical properties, has not been the subject of thorough investigation until quite recently. Lately, photodissociation dynamics of acetyl cyanide at 193 nm have been studied by the Hall[1] and Guest[2] groups. Unimolecular reactions of acetyl cyanide in the ground electronic state are quite complicated, and only several experimental and theoretical studies have been reported so far.[3–5]

Acetyl cyanide has two C–C chemical bonds adjacent to the C═O group, of which the bond characters are expected to be quite different from each other. Therefore, the excited acetyl cyanide can dissociate via two different dissociation pathways as follows; in the case when the internal energies of the COCN or CH_3CO products are higher than their C–C bond dissociation energies, the secondary dissociation takes place to give final fragments.

$$CH_3COCN+h\nu\rightarrow CH_3+COCN^*\rightarrow CH_3+CO+CN,$$

$$CH_3COCN+h\nu\rightarrow CH_3CO^*+CN\rightarrow CH_3+CO+CN.$$

The bond strength of the H_3C–C bond is expected to be weaker than that of the C–CN bond, since the latter has a double-bond character due to a conjugation effect between C═O and C≡N groups. Thus in the energized acetyl cyanide, the weaker H_3C–C bond is expected to be cleaved preferentially over the stronger C–CN bond, as has been demonstrated for some asymmetric aliphatic ketones.[6]

Surprisingly, however, recent photodissociation dynamics studies indicate that the primary dissociation of the acetyl cyanide excited at 193 nm takes place along the C–CN bond exclusively.[1,2] Similar experimental findings have been reported for photodissociation dynamics of acetyl halide molecules.[7–9] The Butler group[7–9] has observed that the CH_3COCl molecule, when it is excited at 248 nm, dissociates primarily into CH_3CO+Cl in spite of the fact that the C–Cl bond is stronger than the C–C bond. This observation has been interpreted to be due to the difference in mechanisms of the C–Cl and C–C bond cleavages in terms of electronic couplings involved in the dissociation processes, and has provided a new way for the bond-selective breakage of polyatomic molecules via selective electronic transitions. Photodissociation dynamics of acetyl cyanide could be similar to those of acetyl halides in terms of electronic couplings involved in the photodissociation dynamics. However, for the acetyl cyanide molecule, the dissociation mechanism is not yet clear, especially since the electronic states involved in the optical transition and dissociation processes are not clearly identified at the present time. Thus the spectroscopic studies of acetyl cyanide along with theoretical and experimental investigations of the photodissociation dynamics occurring on its many different electronic states should be carried out for the better understanding of the nature of the chemical bond dissociation.

Here, as the first stage of the laser spectroscopic study, we report the fluorescence excitation spectrum for the $^1(n,\pi^*)$ transition of acetyl cyanide in the supersonic jet. Even though reliable theoretical values for vibrational frequencies and structural parameters of the S_1 state are not available at the present time, some of the peaks observed in the fluorescence excitation spectrum could be assigned to specific vibrational modes of the S_1 state. The fluorescence lifetimes are also measured as a function of the excitation energy, and from the change of the fluorescence intensity and lifetime with increasing the excitation energy, nonradiative transition processes involving intramolecular vibrational redistribution (IVR) are discussed.

II. EXPERIMENT

Acetyl cyanide (Aldrich +95%) was purchased and used without further purification. The UV absorption spectrum of acetyl cyanide in *n*-hexane solvent was taken using a con-

a)Author to whom correspondence should be addressed; Electronic mail: skkim@inha.ac.kr

ventional UV/VIS spectrometer (Scinco 1.1) with a spectral resolution of 0.8 nm. Acetyl cyanide was kept at room temperature, and the He carrier gas was bubbled through the sample. The gas mixture was then expanded into a vacuum chamber through a nozzle orifice (0.5 mm diameter, General Valve) with a typical backing pressure of 1 atm. The nozzle was operated at a repetition rate of 10 Hz with a homemade driver. The vacuum chamber was equipped with a 6 in. diffusion pump (VHS-6) and a liquid N_2 trap, and the background pressure was maintained at 10^{-5} Torr when the nozzle was on. The nozzle was heated to 70 °C to reduce the cluster formation.

The second harmonic output of a Nd:YAG laser (Spectra-Physics, GCR-150) was used to pump a dye laser (Lambda Physik, Scanmate II) to generate the laser pulse in the 680–740 nm region using LDS698 or LDS751 dyes. The output of the dye laser was frequency doubled via a KD*P crystal placed on a homemade autotracker to give the UV laser output in the 340–370 nm region with a pulse duration of 7 ns and the power of ~1 mJ/pulse. The coherence width was ~0.0007 cm^{-1}, and the spectral line width was ~0.4 cm^{-1}. The laser frequency was calibrated using the optogalvanic signal of a hollow-cathode lamp with an accuracy of ± 0.5 cm^{-1}. The UV laser pulse was directed into the vacuum chamber via three dichroic mirrors, and overlapped with the molecular beam at the position of ~20 mm downstream from the nozzle orifice, providing $x/d = 40$.

The fluorescence was collected by using a 2 in. diameter lens (focal length=5 cm), imaged onto the slit, and detected by a photomultiplier tube (Hamamatzu, H-1949-50). The fluorescence signal was gate-integrated by a boxcar (SRS 250), A/D converted by an interface (SRS 245), and stored in a PC (386, 20 MHz) using a data-taking program, which also controls the dye laser and autotracker system. The signal was averaged for ten laser shots and normalized to the laser intensity fluctuation monitored by a photodiode. Fluorescence lifetimes were measured without using imaging optics in front of the PMT using a 300 MHz digitized oscilloscope (LeCroy 9361).

III. RESULTS AND DISCUSSION

The fluorescence excitation spectrum of acetyl cyanide provides the information about the S_1 state vibrational frequencies of the optically active modes, and one can learn about the rate of nonradiative transitions from the fluorescence lifetime and its quantum yield. Finally, we will discuss the evidence of the intramolecular vibrational redistribution (IVR) process at high vibrational energies occurring within the fluorescence lifetime of the S_1 state.

A. Fluorescence excitation spectrum and assignments

The fluorescence excitation spectrum of the jet-cooled acetyl cyanide for the $^1(n,\pi^*)$ transition is shown with its UV absorption spectrum taken in *n*-hexane solvent in Fig. 1. The origin band is located at 27 511 cm^{-1}, and the relative positions of many transitions from the origin provide the vibrational structure of the S_1 state of acetyl cyanide. The rotational contour analysis shows that there are two types of transitions in the fluorescence spectrum, the *C*- or *AB*-hybrid

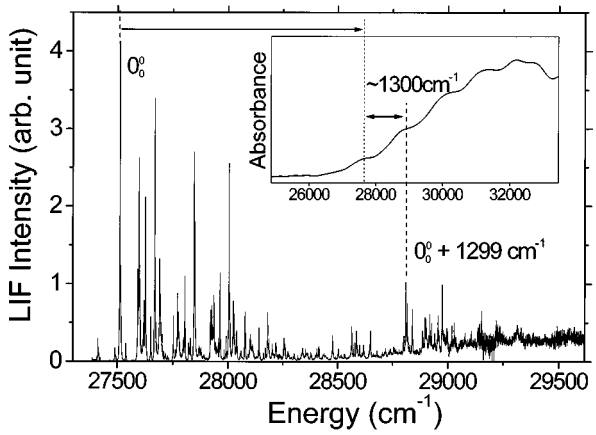

FIG. 1. Fluorescence excitation spectrum of the jet-cooled acetyl cyanide in the 27 500–29 700 cm^{-1} region. The UV absorption spectrum of acetyl cyanide in *n*-hexane solvent is also shown. The spacing between vibronic progressions in the UV absorption spectrum is estimated to be ~1300 cm^{-1}.

types. In Fig. 2, the bands centered at 27 511 and 28 077 cm^{-1} are compared with simulated rotational contours based on selection rules of the *C*- and *AB*-hybrid (5:5) type transitions, respectively, using an asymmetric-rotor simulation program.[10] The simulation has been carried out using experimental rotational constants of *A*, *B*, and $C = 0.340$, 0.1387, and 0.1002 cm^{-1}, respectively, for both the ground and excited electronic states.[11] The best simulation could be obtained at $T = 7$ K. Most transitions observed in the fluorescence excitation spectrum are the *C*-type transitions, indicating that the transition dipole moment for this electronically allowed transition is perpendicular to the molecular plane. The *AB*-hybrid type transitions are only vibronically allowed, and thus their intensities are found to be relatively weak (*vide infra*). One possible mechanism for this vibronic coupling observed here would be Herzberg–Teller intensity borrowing of the n-π^* state from a higher lying π-π^* state with a much larger transition moment.[12] The vibrational modes associated with the *AB*-hybrid type transi-

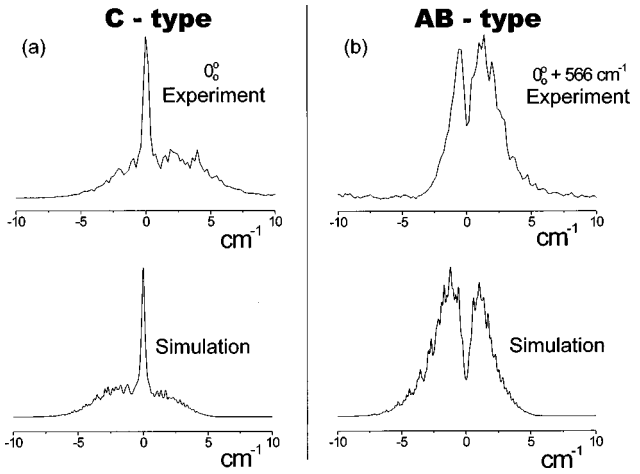

FIG. 2. The experimental and simulated spectra of (a) the *C*-type and (b) the *AB*-hybrid type (5:5) transitions assuming no geometrical change of the S_1 state from the S_0 state. The temperature of 7 K is used in the simulation. See the text for rotational constants used in the simulation.

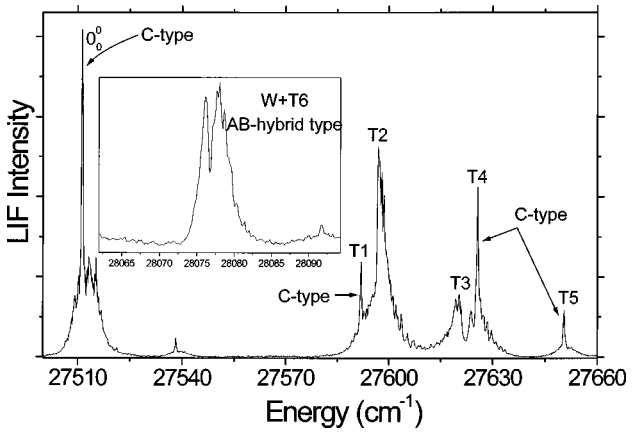

FIG. 3. LIF spectrum of acetyl cyanide in the 27 500–27 660 cm^{-1} region. The bands assigned as the origin, $T1$, $T4$, and $T5$ show *C*-type transitions, while those assigned as $T2$ and $T3$ show neither *C*-type nor *AB*-hybrid type transitions. The band assigned as $W+T6$ is shown in the box just for comparison.

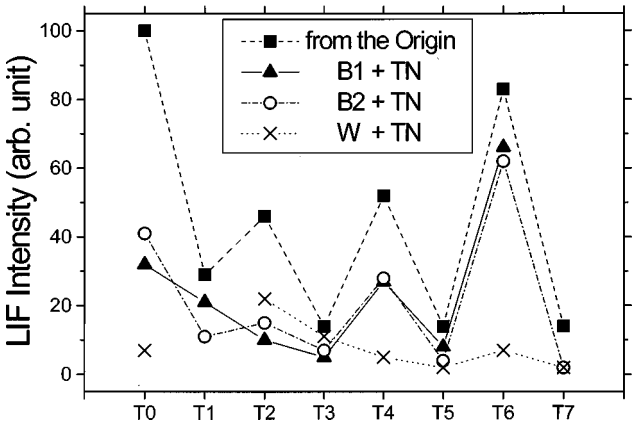

FIG. 4. The fluorescence intensity versus the CH_3 torsional progression number ($T0-T7$). The intensity variation patterns of the torsional progression bands are quite similar for the origin and combination bands with the CCN bend or CCO bend.

tions from the ground state (where the vibronic symmetry is A') should be vibrationally nontotally symmetric, since the vibronic symmetry of the S_1 state is A' while the electronic symmetry of the S_1 state is A''.

The first progression bands observed at 81, 86, 109, 114, 139, 157, and 241 cm^{-1} are assigned to those of the CH_3 torsional mode (a''), and are denoted here, just for convenience, as $T1$, $T2$, $T3$, $T4$, $T5$, $T6$, and $T7$, respectively. It should be noted that the number here is not exact quantum number of the torsional mode. Most of these bands are the *C*-type transitions. Although the torsional mode does vibrationally belong to the a'' symmetry class, due to the tunneling effect through a finite barrier of the internal rotation of the CH_3 moiety with respect to the rest of the molecule, even the zero-point energy level splits into two closely-spaced levels with different symmetries (a,e).[13] Furthermore, in the supersonic jet, both the lowest lying a and e states in the ground electronic state are expected to be populated. Therefore, even though the symmetry of the torsional energy level in the S_1 state changes with increasing the quantum number, most of the spectral intensities should come from the electronically allowed transitions, resulting in the *C*-type transitions. It should be noted however that the shapes of the bands labeled as $T2$ and $T3$ are hardly reproduced, neither from the *C*-type nor from the *AB*-hybrid type transitions (Fig. 3). Thus, their assignments are not conclusive at the present time. It is possible though that these bands are associated with the energy levels coming from the coupling of the internal rotation to the overall rotation of the entire molecule.[14] The observed torsional bands provide the information about the potential shape along the CH_3 torsional angle. However, this analysis requires the accurate molecular structure of the S_1 state which is not available at the present time, and will be investigated in future work.

With this torsional progression, several pseudo origins have been found to be at 178, 337, and 410 cm^{-1}. The experimentally observed vibrational frequencies of CCO. CCN in-plane bending modes, and C═O wagging mode in the ground electronic state are 176, 431, and 535 cm^{-1}, respectively.[15] Upon the $^1(n,\pi^*)$ transition of the C═O moiety as a chromophore, the vibrational modes involving the motion of the C═O group are expected to be relaxed, while those not including the C═O motion are expected to be less affected.[12] Accordingly, the pseudo origins at 178, 337, and 410 cm^{-1} are assigned to fundamentals of vibrational modes associated with CCN bend (a'), CCO bend (a'), and CO wag (a''), respectively, and denoted here as $B1$, $B2$, and W, respectively. The fact that the 410 cm^{-1} band is the vibronically allowed *AB*-hybrid type transition strongly supports that this band is associated with the out-of-plane mode. The assignment of the torsional progression band is checked by plotting the peak intensity versus the torsional progression number. The intensity variation of the torsional progression bands from $T0$ to $T7$, combined with the $B1$, $B2$, and W fundamentals, are compared to that of the torsional progression bands from the origin in Fig. 4. The similar pattern has been observed for all the torsional progression bands except those combined with the C═O wagging mode, suggesting that one quanta of the C═O wag may change the Franck–Condon overlap of the CH_3 torsional bands.

Observed transition wavenumbers, relative shifts from the origin, relative signal intensities, types of transitions, and assignments are summarized in Table I. Many combination or overtone bands of these vibrational modes including the torsional progression are observed. It should be noted here that all the combination bands including ''one'' quanta of the CO wagging mode show the opposite types of transitions to those with ''zero'' quanta of the CO wagging mode. That is, as shown in Table I, were the 410 cm^{-1} band combined with other bands, the *C*-type transition becomes the *AB*-hybrid type transition. This again provides strong evidence for the assignment of the 410 cm^{-1} band to the CO wagging mode. In contrast, combination bands including one quanta of either CCN or CCO bending modes are found to give the same type of transitions as those with zero quanta of those modes, indicating that these are in-plane modes which belong to the a' symmetry class.

Almost all of the peaks from the origin up to ~1000

TABLE I. Vibronic analysis of the $^1(n,\pi^*)$ state of acetyl cyanide.

Transition wavenumber	Δ cm^{-1}	Intensity[a]	Rot. type	Assignment[b]	Difference[c] (cal.−exp.)	τ_F, ns[d]
27 511	0	100	*C*	$0_{0,0}$		3500
27 592	81	29	*C*	*T*1		
27 598	86	24		*T*2		3900
27 620	109	8.2		*T*3		
27 626	114	52	*C*	*T*4		
27 650	139	14	*C*	*T*5		
27 668	157	83	*C*	*T*6		4200
27 690	178	32	*C*	*B*1		
27 752	241	14	*C*	*T*7		
27 770	259	21	*C*	*B*1+*T*1	0	4700
27 775	264	6		*B*1+*T*2	0	
27 798	287	3.5		*B*1+*T*3	0	
27 804	293	27	*C*	*B*1+*T*4	−1	
27 821	310	8	*C*	*B*1+*T*5	7	
27 845	334	66	*C*	*B*1+*T*6	1	3500
27 849	337	44	*C*	*B*2		3600
27 921	410	7	*AB*	*W*		
27 927	415	18	*C*			
27 931	419	11	*C*	*B*2+*T*1	−1	4300
27 936	424	7.8		*B*2+*T*2	−1	
27 956	445	7	*C*	*B*2+*T*3?	1	
27 963	452	28	*C*	*B*2+*T*4	−1	
27 983	471	4	*C*	*B*2+*T*5	5	
27 991	480	8	*C*			
28 004	492	62	*C*	*B*2+*T*6 / *W*+*T*1	2/−1	3400
28 007	495	22		*W*+*T*2	1	
28 023	512	19	*C*	*B*1+*B*2	3	
28 027	515	11		*W*+*T*3	4	
28 039	527	4	*AB*	*W*+*T*4	−1	
28 059	548	1.3	*AB*	*W*+*T*5	1	
28 077	566	6	*AB*	*W*+*T*6	1	
28 092	581	2	*C*	*B*2+*T*7	−3	
28 100	589	3	*AB*	*W*+*B*1	−1	
28 141	630	11	*C*	*B*1+*B*2+*T*4	−4	
28 161	650	3	*C*	*W*+*T*7	1	
28 170	659	4	*C*			
28 181	669	13	*C*	*B*1+*B*2+*T*6	0	4400
28 186	675	7	*C*	2*B*2	−1	
28 201	689	6	*C*			
28 208	697	2		*W*+*B*1+*T*3	1	
28 218	707	2.6	*AB*	*W*+*B*1+*T*4	−4	
28 255	741	3.5	*AB*			
28 258	747	2.2	*AB*	*W*+*B*2 or *W*+*B*1+*T*6	0/−1	
28 273	761	3	*C*			
28 302	790	3	*C*			
28 319	807	2	*C*			
28 339	828	1.7	*AB*	*W*+*B*2+*T*1	0	
28 344	832	3		*W*+*B*2+*T*2	1	
28 353	842	4	*C*			
28 359	848	1.3	*AB*			
28 364	852	3		*W*+*B*2+*T*3	4	
28 377	866	1.3	*AB*	*W*+*B*2+*T*4	−5	
28 405	894	4	*C*			
28 414	903	2.2	*AB*	*W*+*B*2+*T*6	1	
28 437	926	1.3	*AB*	*W*+*B*1+*B*2	−1	
28 476	965	8	*C*			
28 502	991	4	*C*			
28 504	993	4	*C*			
28 564	1053	11	*C*	C–CN str.		
28 574	1063	6	*C*			
28 584	1072	8	*C*			
28 586	1075	10	*C*			
28 600	1089	5	*C*			
28 613	1101	3	*C*			

TABLE I. (*Continued.*)

Transition wavenumber	Δ cm^{-1}	Intensity[a]	Rot. type	Assignment[b]	Difference[c] (cal.–exp.)	τ_F, ns[d]
28 618	1107	5	*C*			
28 646	1135	5	*C*	C–CN str.+*T*1	−1	
28 650	1138	6		C–CN str.+*T*2	−1	
28 679	1168	1.7		C–CN str.+*T*4	−1	
28 704	1192	3	*C*	C–CN str.+*T*5	0	
28 719	1207	4	*C*	C–CN str.+*T*6	4	
28 740	1229	4	*C*	C–CN str.+*B*1	2	
28 755	1244	5	*C*			
28 810	1299	25	*C*	C═O str.		
28 817	1305	18	*C*			
28 828	1317	2.2	*AB*			
28 840	1328	17	*C*			
28 886	1374	10	*C*	C–CN str.+*B*2?	16	
28 898	1387	14	*C*			
28 919	1408	15	*C*			
28 928	1416	12	*C*			
28 942	1430	4	*AB*			
28 956	1445	15	*C*			
28 975	1464	24	*C*			
28 997	1486	5	*AB*			

[a]Relative intensities when the intensity of the origin band=100.
[b]*T*: CH_3 torsion, *B*1: CCN bend, *B*2: CCO bend, *W*: C═O wag.
[c]The difference between the experimental and calculated values without considering anharmonicities.
[d]Uncertainties are within ±10%.

cm^{-1} could be nicely assigned with four low-frequency fundamentals associated with CH_3 torsion, CCO bend, CCN bend, and CO wag. The torsional progression bands combined with the 1053 cm^{-1} band are also clearly identified (see Table I). This 1053 cm^{-1} band is tentatively assigned to the C–C(N) stretching mode just from the similarity in the number with the 1178 cm^{-1} for the same mode in the ground electronic state.[15] A relatively strong band observed at 1299 cm^{-1} is likely due to the C═O stretching mode. In the $^1(n,\pi^*)$ transition, the C═O bond is expected to be lengthened due to the promotion of a nonbonding electron to the antibonding π^* state along the C═O bond. Thus, the C═O stretching mode should be Franck–Condon active in the fluorescence excitation spectrum. Actually, in the UV absorption measurement of acetyl cyanide in *n*-hexane solvent, a vibronic progression, though it is not clearly resolved, has been observed with a spacing of ~1300 cm^{-1} as shown in Fig. 1. The torsional progression bands combined with the 1299 cm^{-1} band are not clearly assignable with a simple arithmetic method that has been used for the other fundamental bands, possibly due to a severe coupling among vibrational modes at the relatively high vibrational energy region (*vide infra*).

B. Nonradiative transitions

The fluorescence lifetime has been measured for several transitions, and listed in Table I. The fluorescence lifetime of the origin band is 3.5±0.3 μs (Fig. 5). As the energy increases from the origin to 1500 cm^{-1}, the fluorescence lifetime changes little to give τ_F=3.2~4.7 μs for most of bands in the 0–1500 cm^{-1} region above the origin (Table I). The fluorescence lifetime does not show any particular mode dependence. The modest change of the fluorescence lifetime with increasing the vibrational energy indicates that the nonradiative transition rate changes little in the 0–1500 cm^{-1} region of the S_1 state, excluding the possibility of any fast vibrational or electronic predissociation processes in the corresponding energy range. Therefore, the nonradiative transition is likely due to internal conversion or intersystem crossing to the S_0 or T_1 states, of which the rates are expected to vary quite slowly within the 0–1500 cm^{-1} region above the origin, since the density of states at highly vibrationally excited states in the S_0 or T_1 state is not expected to be a sharply varying function of the energy[14,16] in the relatively small range of the energy investigated in this work.

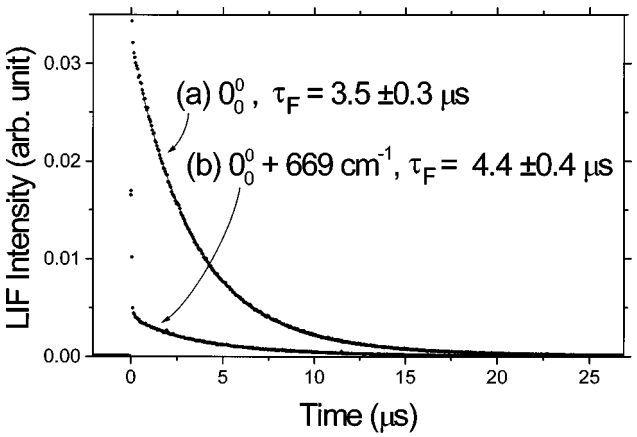

FIG. 5. The fluorescence decay curves of (a) the origin and (b) the origin +669 cm^{-1} bands. The single exponential fits give τ_F=3.5±0.3 and 4.4 ±0.4 μs for (a) and (b), respectively. The fluorescence intensities are arbitrarily rescaled for the comparison.

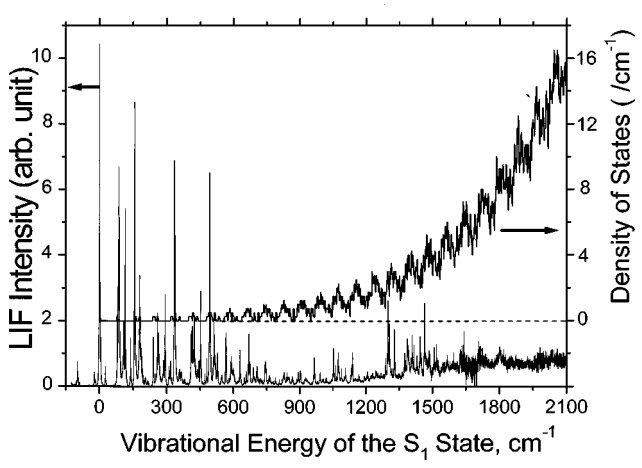

FIG. 6. The plot of $\rho_{\mathrm{vib}}(E)$ versus the vibrational energy of the S_1 state. The fluorescence excitation spectrum is also shown in the same energy region for the comparison. As $\rho_{\mathrm{vib}}(E)$ increases, the apparent fluorescence intensity decreases and a broad background signal rises and persists in the high energy region.

C. Intramolecular vibrational redistribution (IVR)

The dramatic decrease of the fluorescence intensity with increasing the energy is observed, while the absorption coefficient seems to increase for the same energy region in the UV absorption spectrum (Fig. 1). Were this fluorescence intensity taken to be Φ_{F}, then from $\Phi_{\mathrm{F}}=k_{\mathrm{R}}/(k_{\mathrm{R}}+k_{\mathrm{NR}})$ and $\tau_{\mathrm{F}}=1/(k_{\mathrm{R}}+k_{\mathrm{NR}})$, a sharp decrease of the fluorescence lifetime is expected, possibly due to the opening of a new decay channel.[17] However, as described above, the fluorescence lifetime changes little in the energy region where the apparent fluorescence quantum yield decreases quite rapidly. This suggests that the intramolecular vibrational redistribution (IVR) process may take place as the density of the S_1 states increases with increasing the energy. Actually, as the energy increases, the broad background signal starts to appear and persists in the high energy region (Fig. 1). The fluorescence lifetime of the background signal is also measured to be around $3.2\sim4.7\ \mu$s, which indicates that the background signal is less likely due to impurities or clusters, which would probably give different lifetimes. The appearance of the background signal suggests that the S_1 dark states may be strongly coupled with optically bright states through an efficient IVR process. The IVR process occurs typically on the subnanosecond time scale,[18–20] and the fluorescence lifetime of $\sim4\ \mu$s of the excited acetyl cyanide ensures a sufficiently long time for the optically prepared S_1 states to undergo the energy randomization among isoenergetic dark states.

The density of the S_1 states, $\rho(E)$, has been calculated using the experimentally observed vibrational frequencies for the CH_3 torsional progression, CCN bend, CCO bend, C–C(N) stretching, and C═O stretching modes. Just for convenience, the value of 80 cm^{-1} is used for the CH_3 torsional mode in the calculation of the density of states. For the vibrational frequencies of the remaining modes, those of the ground electronic state have been used.[15] The density of states is calculated using the Beyer–Swinehart algorithm[21] assuming harmonic oscillators for all the S_1 state vibrational modes. In Fig. 6, the density of states is plotted versus the vibrational energy of the S_1 state over the 0–2100 cm^{-1} region with the fluorescence excitation spectrum. Since the size of the acetyl cyanide molecule is medium, the increase of $\rho(E)$ is not dramatic in the relatively low energy region. For example, $\rho(E)=3.5$ and $12/\mathrm{cm}^{-1}$ at 1500 and 2000 cm^{-1}, respectively. Nevertheless, as shown in Fig. 6, the density of states is found to increase rapidly starting at around ~1000 cm^{-1}, and this coincides with the energy where the fluorescence intensity starts to decrease and the background signal starts to increase. Furthermore, the unassignable peaks located above 1000 cm^{-1} (see Table I) seem to reflect the energy dependent structure of $\rho(E)$. At vibrational energies above ~1500 cm^{-1}, no sharp structure is observed in the fluorescence excitation spectrum, suggesting the complete IVR among the S_1 states at those high energies.

The reason why the IVR process is observed quite early in the relatively low energy region of this medium-sized molecule is probably that the fluorescence lifetime is sufficiently long enough for the IVR process, even with a small rate constant, to occur efficiently. The estimation of the IVR rate constant is not plausible in the present work. The higher resolution spectroscopic study or the ultrafast real time probing of the emission would be quite helpful for further investigation of the IVR dynamics of the S_1 state of acetyl cyanide. The measurement of dispersed fluorescence spectra would also be quite helpful for understanding the IVR dynamics and the more accurate assignments of the S_1 bands. The work is on the way in our laboratory along this direction.

IV. CONCLUSIONS

Here, we report the fluorescence excitation spectrum of the jet-cooled acetyl cyanide molecule for the $^1(n,\pi^*)$ transition. The origin is located at 27 511 cm^{-1}, and low frequency vibrational modes associated with the CH_3 torsion, CCN bend, CCO bend, and C═O wag are found to be optically active. The fluorescence lifetime is found to be ~3.5 μs for the origin band, and it changes little over the 0 $\sim2000\,\mathrm{cm}^{-1}$ region above the origin. As the energy increases, the fluorescence intensity decreases. Instead, a broad background starts to appear and persist in the high energy region. This implies that the IVR process becomes quite efficient as the density of the S_1 states increases. The long lifetime of the S_1 state ($3.2\sim4.7\ \mu$s) seems to be responsible for the complete IVR in the high energy region, resulting in no sharp structure in the fluorescence spectrum at the vibrational energies higher than ~1500 cm^{-1}.

ACKNOWLEDGMENT

The authors are grateful to Professor Byung-Seo Chung for helpful discussions. This work has been financially supported by Korea Science and Engineering Foundation (Project No. 971-0305-037-2) and Korea Research Foundation (Project No. 1998-001-D00425).

[1] S. W. North, A. J. Marr, A. Furlan, and G. E. Hall, J. Phys. Chem. A **101**, 9224 (1997).
[2] R. J. Horwitz, J. S. Francisco, and J. A. Guest, J. Phys. Chem. A **101**, 1231 (1997).

[3] S. P. So, Chem. Phys. Lett. **270**, 363 (1997).
[4] K. Okada and K. Saito, J. Phys. Chem. **99**, 13168 (1995).
[5] R. Sumathi and M. T. Nguyen, J. Phys. Chem. A **102**, 412 (1998).
[6] J. G. Calvert and J. N. Pitts Jr., *Photochemistry* (Wiley, New York, 1966), p. 379.
[7] M. D. Person, P. W. Kash, and L. J. Butler, J. Phys. Chem. **96**, 2021 (1992).
[8] M. D. Person, P. W. Kash, and L. J. Butler, J. Chem. Phys. **97**, 355 (1992).
[9] G. C. G. Waschewsky, P. W. Kash, T. L. Myers, D. C. Kitchen, and L. J. Butler, J. Chem. Soc., Faraday Trans. **90**, 1581 (1994).
[10] F. W. Birss and D. A. Ramsay, Comput. Phys. Commun. **38**, 83 (1984).
[11] L. C. Krisher and E. B. Wilson, J. Chem. Phys. **31**, 882 (1959).
[12] M. Baba, I. Hanazaki, and U. Nagashima, J. Chem. Phys. **82**, 3938 (1985).
[13] W. J. Orville-Thomas, Ed., *Internal Rotation in Molecules* (Wiley, London, 1974).
[14] S. K. Kim, E. R. Lovejoy, and C. B. Moore, J. Chem. Phys. **102**, 3202 (1995).
[15] M. Sugie and K. Kuchitsu, J. Mol. Struct. **20**, 437 (1974).
[16] W. H. Green, C. B. Moore, and W. F. Polik, Annu. Rev. Phys. Chem. **43**, 591 (1992).
[17] E. K. C. Lee and R. S. Lewis, Adv. Photochem. **12**, 1 (1980).
[18] L. R. Khundkar and A. H. Zewail, Annu. Rev. Phys. Chem. **41**, 15 (1990).
[19] C. S. Parmenter, Faraday Discuss. Chem. Soc. **75**, 7 (1983).
[20] R. E. Smalley, J. Phys. Chem. **86**, 3504 (1982).
[21] R. G. Gilbert and S. C. Smith, *Theory of Unimolecular and Recombination Reactions* (Blackwell, Oxford, 1990).